Chapter 4
Photocatalytic Degradation of Aqueous Organic Pollutants Using Iron Oxide-Based Photocatalysts

Yagna Prakash Bhoi and Weixin Huang

Abstract Pollution of water bodies arose due to invade of pollutants from various sector of society such as industries, agricultural field and domestic effluent water, etc. Heavy metals, pathogens and recalcitrant organic chemicals are typical examples of deleterious elements that adversely affect the health of aquatic environment. The removal of such pollutants has become an urgent need across the globe, which brings the discovery of various water treatment techniques in order to get clean water. In past few decade, outstanding result has been achieved in the field of water desalination. The application of heterogeneous photocatalysis route for the cleaning of water is reflected as one of the potential and sustainable approach since it makes use of renewable solar light as source of energy. In this chapter, we will discuss the application of iron oxide-based photocatalysts towards the removal of pollutants from aqueous source. Various research approaches progressed to improve the photocatalytic ability of iron oxide will be discussed in detail. The discussion of this chapter particularly focussed on the evolution of composite/heterostructure of iron oxide-based photocatalysts and their photocatalytic applications towards the removal of aqueous pollutants.

Keywords Photocatalysis · Water pollutant · Solar energy · Iron oxide nanocomposite

4.1 Introduction

The water pollution and its impact on the all life on the earth is a global concern. The discharged water from the chemical and agrochemical industries contains substantially huge amount of toxic and carcinogenic organic chemicals such as VOC, pesticides, dyes, etc., which infused into water bodies. This water pollution is one of the

Y. P. Bhoi (✉) · W. Huang
Hefei National Laboratory for Physical Sciences at Microscale, Department of Chemical Physics, University of Science and Technology of China, Jinzhai Road 96, Hefei 230026, P.R. China
e-mail: yagnapbhoi@gmail.com

H. Sahoo and J. K. Sahoo (eds.), *Iron Oxide-Based Nanocomposites and Nanoenzymes*, Nanostructure Science and Technology, https://doi.org/10.1007/978-3-031-44599-6_4

responsible factor for many water-borne diseases and scarcity of portable water. In this perspective, development of low-cost and high efficient water treatment technologies to treat and recycle the wastewater in a sustainable way is prime importance in order to get portable water for our society. Various methodologies were developed in recent past, which includes wet air oxidation, UV photolysis, adsorption and biodegradation methods are available for wastewater treatment [1–3]. The adsorption or coagulation techniques are among the widely used desalination technique in order to remove organic and inorganic pollutants from contaminated water [2]. However, these techniques simply concentrate the pollutants by transferring them to other phases. Sedimentation, filtration, chemical and membrane technologies are some examples of some conventional water treatment techniques, which suffers with the limitations like high operational cost and could produce toxic by-products into the environment. It is highly essential to develop advanced water treatment technology, which can mineralize the organic pollutants completely by a simple and easy experimentation process, less expense of energy and cost. In this perspective, the complete mineralization of organic pollutants by heterogeneous photocatalytic process using solar light as energy source and semiconductor nanoparticles as catalyst is a sustainable strategy to deal.

4.2 Fundamental of Photocatalysis

Photocatalysis is the science, which employed a catalyst and light as energy source to speed up chemical reactions and photocatalyst is a material that is capable of absorbing light, producing electron–hole pairs that enable chemical transformations of the reactants and regenerate after each cycle. When light energy with greater than the band gap energy (E_g) of the photocatalyst falls on the photocatalyst surface, the electron gets excited to the conduction band (CB) leaving a hole in the valance band (VB). The electron hole migrates to the surface of the photocatalyst and participate in reaction with different substrate. On the other hand, some of the electron hole recombines themselves, which leads to the poor photocatalytic activity of the catalyst (Fig. 4.1). The splitting of water by Fujishima and Honda over TiO_2 surface in the presence of light and electricity put the foundation for the semiconductor-based photocatalysis [4]. Until now TiO_2 is the most widely studied photocatalyst with promising field of applications such as environmental cleaning, self-cleaning surfaces, air and water purification, sterilization, hydrogen evolution, and photoelectrochemical conversion of energy, etc. [4]. TiO_2 is a wide band gap photocatalyst with band gap of 3.2 eV. Although, TiO_2 photocatalyst possess advantages such as high oxidation ability, excellent chemical stability, nontoxicity and inexpensive, it suffers limitations like fast recombination of photogenerated electron–hole pair and poor utilization of solar spectrum [4, 5]. Moreover, the solar spectrum comprises only 5–7% of UV light, while 46% and 47% of the solar spectrum has visible light and infrared radiation, respectively [6].

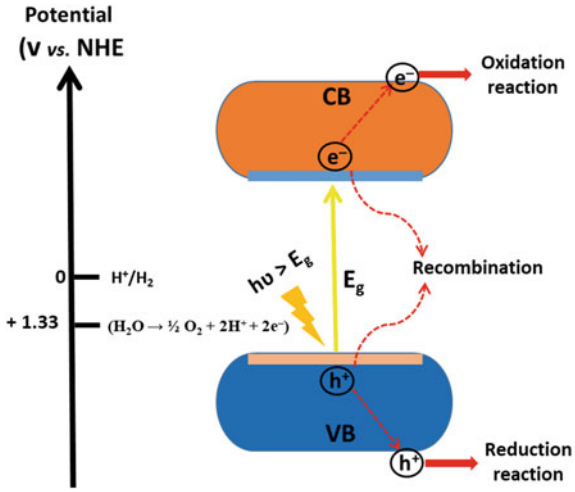

Fig. 4.1 General schematic representation for the working principle of a photocatalyst

In recent past, several research efforts has been put in order to design photocatalyst, which can able to absorb visible light of solar spectrum. MoS_2, CdS, Fe_2O_3, Bi_2WO_6, $Bi_2W_2O_9$, $BiFeO_3$ and bismuth oxyhalides (BiOX, X = Cl, Br, I) are few examples of metal oxide and metal sulphide-based visible light active photocatalyst widely studied for the degradation of a wide range of harmful aqueous organic pollutants into CO_2 and H_2O [7–13]. The pristine photocatalysts suffers with a poor separation of charge carriers, which leads to a poor photocatalytic efficiency of the photocatalysts. With time, noticeable research attempts have been devoted in order to minimize the recombination process of charge carriers and to enhance the light absorption ability of the photocatalyst, by adopting several strategies such as decoration of noble metal nanoparticles over photocatalyst surface, doping, and composite/heterojunction formation by coupling with suitable a semiconductor [14, 15]. Fe_2TiO_5/α-Fe_2O_3/TiO_2, α-NiS/Bi_2O_3, Bi_2S_3/$BiFeO_3$, CuS/$Bi_2O_2CO_3$, Bi_3S_3/β-Bi_2O_3/$ZnIn_3S_4$, CuS/$BiFeO_3$, CuS/$Bi_4Ti_3O_{12}$, Bi_2S_3/$Bi_2W_2O_9$, CuS/$Bi_2W_2O_9$, Bi_2O_3/$CuBi_2O_4$, UiO-66/$CdIn_2S_4$, SnS_2/$Bi_4Ti_3O_{12}$, CdS/BiOBr/$Bi_2O_2CO_3$ and CdS/$Bi_{20}TiO_{32}$/$Bi_4Ti_3O_{12}$ are few examples of recently studied heterojunction photocatalytic systems with improved light absorption and charge carrier separation ability [12, 16–27].

4.3 Iron Oxide-Based Photocatalyst

The iron oxides are composed of Fe and O. Among eight different form of iron oxides, the hematite (α-Fe_2O_3), magnetite (Fe_3O_4) and maghemite (γ-Fe_2O_3) are widely studied oxides due to their unique biochemical, magnetic and catalytic properties. The Fe_2O_3 exists in three of different crystalline structures, such as hematite (α-Fe_2O_3), maghemite (γ-Fe_2O_3) and ε-Fe_2O_3 [6, 28]. The α- and γ-phases are extensively studied materials, while β-Fe_2O_3 phase is less studied material because of

the difficulty in the preparation of single-phase material. Rhombohedral–hexagonal α-Fe_2O_3 is highly stable and has significant potentials in photocatalytic applications, as it is nontoxic, inexpensive, earth abundance, corrosion resistance property with a suitable band gap value ($E_g = 2.0–2.2$ eV) to harvest visible light of the solar spectrum, whereas the maghemite is a metastable phase between hematite and magnetite. It has similar crystal structure as magnetite and chemical composition similar to hematite. In the hematite crystal structure, iron occupies the octahedral sites where oxygen is hexagonally close packed. On the other hand in both maghemite and magnetite, iron present in both octahedral and tetrahedral sites and oxygen cubically close packed. The ε-Fe_2O_3 is a transition phase between hematite and maghemite, which attract research attention owing to its unique magnetic properties. Seeing the extensively used of both hematite and maghemite form of Fe_2O_3 than the other polymorphs, this study is focussed on their utilizations in the field of heterogeneous photocatalysis towards the degradation of various persistent organic contaminants from aqueous medium.

Song and co-worker prepare α-Fe_2O_3 nanodisks by the assembly of single-crystalline nanoplates with layered structures by using a silicate-anion-assisted hydrothermal method. The silicate anions believe to adsorb selectively onto the {0001} plane of α-Fe_2O_3 nanoplates and induce the self-assembly of the plates to give the layered nanodisks structure. The α-Fe_2O_3 nanodisks display enhanced visible light absorption with excellent photocatalytic activity for the degradation of methylene blue under visible light irradiation [29]. Heidari and co-worker reported the synthesis of porous network-like α-Fe_2O_3 and α/γ-Fe_2O_3 nanoparticles by a simple solution combustion method and evaluated the photocatalytic activity towards the degradation of methylene blue (MB) dye under. The Fe_2O_3 materials calcined at 700 and 800 °C contains diffraction peaks for only α-Fe_2O_3, where Fe_2O_3 material obtains after a calcination at 450 °C, which contains both the α and γ-Fe_2O_3 for of Fe_2O_3. The higher photocatalytic efficiency of the α/γ-Fe_2O_3 heterophase material may be account for the formation of junction between α-Fe_2O_3 and γ-Fe_2O_3 phases, which reduced the recombination of photogenerated electrons, and holes [30]. Jing and co-workers studied the photocatalytic activity of pure α-Fe_2O_3 as well as phosphate-modified α-Fe_2O_3. They have employed the simple one-pot water-organic two-phase separated hydrolysis-solvothermal (HST) method for the preparation of α-Fe_2O_3 nanoparticles. The phosphate-modified α-Fe_2O_3 exhibits high visible photocatalytic activity for the degradation of liquid-phase phenol and gas-phase acetaldehyde. After surface modification with phosphate, the surface –Fe–OH substituted with –Fe–O–P–OH groups, which significantly promote O_2 adsorption over the catalyst surface. The enhanced photocatalytic activity is due to the enhancement in charge carriers separation ability after the modification with phosphate groups [31]. By using electron beam evaporation through a normal thin film deposition and oblique angle deposition (OAD), Fe_2O_3 thin films and nanorod arrays fabricated by Larsen and co-workers [32]. The growth of the materials aligns towards the (110) direction. Under visible light, the Fe_2O_3 thin film samples shows more photocatalytic efficiency towards the degradation of methylene blue dye. Whereas the Fe_2O_3 nanorod inactivate more efficiently to the *Escherichia coli* O157:H7 bacteria as compared to

the Fe_2O_3 thin films. Bahnemann and co-workers demonstrated the generation of H_2O_2 species during the photocatalytic oxidations of organic compounds by using α-Fe_2O_3 photocatalyst. In a comparison study, the ZnO and TiO_2 photocatalysts found to be more active in the generation of H_2O_2 and in the degradation of chlorinated hydrocarbon molecules as compared to the α-Fe_2O_3 photocatalyst [33]. Hameed and co-workers successfully fabricated the α-Fe_2O_3 and γ-Fe_2O_3 polymorphs by using a simple surfactant (Triton X) aided hydrogel synthetic route. The photocatalytic properties of both the form of Fe_2O_3 were studied for the mineralization of 2-chlorophenol and 2-nitrophenol pollutants under the visible light as well as under natural sunlight illumination. Both the polymorphs showed a considerably high activity for the degradation of the phenolic compounds under solar light as compared to visible light irradiation. A significant improvement in the photocatalytic activity under visible light was noticed when the polymorphs were pre-exposed to sunlight preceding to the photocatalytic tests. The higher photocatalytic activity of the exposed polymorphs as compared to the unexposed one is due to the introduction of defects sites which traps the excited electrons during the photocatalysis mechanism [34]. Wang and co-workers fabricated a dodecahedral α-Fe_2O_3 nanoparticle with 6 (012) and (104) exposed facets, respectively. The coexistence of these different facets account for a better photocatalytic ability in comparison with the crystals having single exposed facet. They have also demonstrated that the separation of charge carriers between anisotropic facets also has a significant contribution on photocatalytic degradation of Rhodamine B and methylene blue organic dyes [35]. Ramakrishna and co-workers prepared pure α-Fe_2O_3 with nanobraids and nanoporous like structures using an electrospinning synthesis method followed by annealing at 500 °C for 5 h. Both of the nanobraids and nanoporous display excellent photocatalytic degradation activity for Congo red dye with 91.2% and 90.2% degradation, respectively after 140 min of irradiation under visible light. They have demonstrated the significant role of porous surface and small particle size of the α-Fe_2O_3 towards the excellent photocatalytic activity. The superoxide radicals ($O_2^{\cdot -}$), H^+ ion, hydroperoxyl radicals ($^{\cdot}HO_2$), hydroxyl radicals are generated by the reaction of water and oxygen on the photogenerated hole and electron are responsible for the degradation of Congo red dye over the photocatalyst surface [36]. Zheng and co-workers successfully fabricated dendritic α-Fe_2O_3 nanostructures with controlled dimension and morphology by a facile solvothermal synthesis method in the presence of 1-N-butyl-3-methylimidazolium benzoate ([Bmim][PhCOO]) ionic liquid. A change in the molar ratio of [Bmim][PhCOO] to $K_3[Fe(CN)_6]$ from 0:1 to 2:1, and 5:1 can bring the dendrite structure to hexagonal nanoplates and rods. The ionic liquid plays a crucial role in deciding the formation of α-Fe_2O_3 with different morphologies. The α-Fe_2O_3 with rod morphology exhibit superior photocatalytic activity towards visible light-induced degradation of Rhodamine B (RhB) dye as compared to the dendrites and plates structured α-Fe_2O_3 materials. The degree of crystallinity and exposed crystal facets of α-Fe_2O_3 materials accounts for improving the photocatalytic activity [37].

Song and co-workers recently fabricated a snowflake-like α-Fe_2O_3 materials by using a simple single-step hydrothermal approach and studied there photocatalytic activity towards the degradation of a wide variety of organic pollutants such as crystal violet, Rhodamine 6G, methyl orange, etc. The α-Fe_2O_3 snowflakes exhibit a superior photocatalytic activity towards degrading cationic organic dyes (crystal violet, Rhodamine 6G) than for the anionic dye (methyl orange) degradation [38]. Shim and co-workers synthesized porous natured Fe_2O_3 nanorod by a two-step process. First ferrous oxalate dihydrate ($FeC_2O_4{\cdot}2H_2O$) precursor synthesized by a chemical solution processes and second the ferrous oxalate dehydrate on annealing in air at 500 °C for 2 h to get the porous Fe_2O_3 nanorod. The ferrous oxalate dihydrate nanorods precursor has the length 3–9 μm and diameter of between 110 and 150 nm. After thermal annealing, the nanorods structured remain intact in the Fe_2O_3 materials. The Fe_2O_3 nanorod exhibited excellent photocatalytic degradation ability for a wide range of organic pollutants such as RhB, methylene blue (MB), p-nitrophenol (pNP), eosin B and methyl orange (MO), respectively. The porous structures believe to provide more active reaction sites and also facilitates the efficient separation of photogenerated electrons and holes which is accountable for the excellent photocatalytic efficiency of the prepared porous Fe_2O_3 nanorods [39]. Zhou and co-workers has prepared γ-Fe_2O_3 nanoparticles with spherical morphology by using an oxidizing environment via a solution synthesis method by changing the pH and reaction temperature. The spherical nanoparticles has a particle size around 17–55 nm and a BET surface area of 14.357 m^2/g. The pH of the reaction media crucially influence the particle size of the nanomaterials. With increase in the pH value from 6 to 12, the particle size also increases. The as-synthesized γ-Fe_2O_3 nanoparticles show potential photocatalytic activity towards the degradation of Orange I dye under UV and visible light illumination. The γ-Fe_2O_3 nanoparticles prepared at pH 6 at a reaction temperature 60 °C with smallest particle size show highest photocatalytic efficiency than other synthesized γ-Fe_2O_3 nanoparticles [40]. Fardood and co-workers synthesized hematite (α-Fe_2O_3) nanoparticles by a simple, environment-friendly and less-expensive sol–gel synthesis method in the presence of a bio template (Arabic gum). The average particle size of the prepared materials is 45–50 nm. The α-Fe_2O_3 materials evaluated as a potential photocatalyst with a photocatalytic activity of 90% degradation of Congo red dye after a 90 min of irradiation time [41]. Wang and co-workers fabricated hollow microspherical α-Fe_2O_3 nanostructure material by ionic liquid-assisted solvothermal method followed by calcination at 250 °C for 6 h. The α-Fe_2O_3 have a specific surface area up to 220 m^2/g. The α-Fe_2O_3 microspheres show excellent photocatalytic activity towards the degradation of Rhodamine B dye. The as-synthesized α-Fe_2O_3 microspheres exhibit a photocatalytic activity 2–3 times higher than the α-Fe_2O_3 nanoparticles. The higher specific surface area, porous nature and hollow nanostructure play crucial role in the enhanced photocatalytic activity of the α-Fe_2O_3 microspheres [42]. Zhu and co-workers prepared hierarchical α-Fe_2O_3 hollow microspheres using a surfactant-free solvothermal synthesis method and post-thermal treatment at 450 °C for 2 h. The prepared photocatalyst evaluated as a potential catalyst for the degradation of salicylic acid under UV light irradiation [43]. Wang and co-workers fabricated α-Fe_2O_3 nanospheres/microsphere by using

a surfactant and template-free two-step synthesis procedure, hydrothermal treatment followed by a thermal decomposition. The α-Fe_2O_3 nanospheres/microsphere composed of interlinked elongated nanoparticle and nanospheres/microsphere has a diameter around 5 μm, and the elongated particle size is below 30 nm. The α-Fe_2O_3 nanospheres/microsphere is mesoporous in nature, with a pore size distribution between 2 and 50 nm with specific surface area of 20 m^2/g. The photocatalytic activity of the as-synthesized α-Fe_2O_3 nanospheres/microsphere evaluated for the degradation of Rhodamine 6G dye under visible light illumination. The α-Fe_2O_3 nanospheres/microsphere exhibit a photocatalytic efficiency 2 times that of nano-sized α-Fe_2O_3 particles and around 12 times higher than the micron-sized particles. The higher photocatalytic activity of the α-Fe_2O_3 nanospheres/microsphere was due to combined contribution of the high specific surface area and the porous architecture [44]. Wang and co-workers develop a facile solvothermal route to prepare 3D porous flower-like α-Fe_2O_3 nanomaterial with hierarchical architecture without using any structural templates. Two-dimensional α-Fe_2O_3 nanopetals organize themselves in a hierarchical fashion in order to give the 3D porous flower-like structure. The depth morphological analysis reveals that the nanopetals has a thickness between 20 and 50 nm and width of 300–500 nm; moreover, these nanopetals composed of nanobricks with 100 nm in length and 30 nm in diameter. The 3D α-Fe_2O_3 materials has high specific surface area (∼ 52.51 m^2/g) with the presence of numerous mesopores and macropores that facilitate the efficient transportation of the substrate during the catalytic reaction. The photocatalytic activity of the 3D α-Fe_2O_3 nanomaterial explored by the mineralization of Rhodamine B dye under UV light irradiation [45]. Geng and co-workers prepared α-Fe_2O_3 with flue-like 3D porous nanoarchitectures by using a Ni^{2+}/surfactant-assisted solvothermal method at 200 °C for 24 h. The α-Fe_2O_3 material has a specific surface area of 88.82 m^2/g with potential photocatalytic activity towards the degradation of methylene blue dye under visible light. They have closely demonstrated the influence of the Fe^{3+} and Ni^{2+} ion ratio on the morphology of the α-Fe_2O_3 materials. At a molar ratio of Fe^{3+} to Ni^{2+} ion at 1:2 in the solution gives rise to a micro-balls constituted of fine α-Fe_2O_3 nanorods, while at molar ratio of 1:3 gives the 3D flue-like structure and the micro-balls structure again regain on further changing in the molar ratio to 1:4. The 3D flue-like α-Fe_2O_3 shows highest photocatalytic ability for the degradation of methylene blue dye as compared α-Fe_2O_3 nanoparticles and P25 photocatalyst under visible light illumination [46]. The pristine Fe_2O_3 photocatalyst has some limitations such as rapid recombination of photogenerated electron–hole pair and poor response to solar spectrum, which result in poor photocatalytic performances. Within short span of time, a lot of research effort have been devoted to prepare novel hybrid materials such as modification with noble metal, doping and formation of binary and ternary composite/heterojunction material. These strategies believe to suppress the recombination process of charge carriers and enhance the light photocatalytic efficiency as a whole. In the subsequent text, we will discussed the hybrid, doped and noble metal-modified Fe_2O_3 photocatalyst and their photocatalytic applications.

Generally, doping of foreign elements (metal or non-metal) significantly alter the physical parameters, chemical reactivity and redox behaviour of the host material. The doping with non-metal such as nitrogen and sulphur widely studied. The main purpose of non-metal doping in Fe_2O_3, TiO_2 or with metal oxide photocatalysts is to alter the band gap value by mixing the oxygen 2p orbital with that of non-metal. The doping of non-metals believe to creating a trap state (separate band) in between the valence band and conduction band which controls the electron–hole recombination and delay the recombination process so that the photogenerated electron–hole pair could be available for the redox reaction. Parida and co-workers prepare α-Fe_2O_3 material co-doped with S and N by using co-precipitation method. They have used thiourea both as precipitating agent and as the sulphur and nitrogen source. The S and S–N co-doping induced growth along the (104) plane, whereas the N doping induced along the (110) crystal plane. After S and N doping, the specific surface area increases significantly than the un-doped pristine α-Fe_2O_3; on the other hand, the highest surface area has been noticed for the S–N co-doped sample (57.85 m^2/g). This observation indicates the significant contribution of minute amount of sulphate ion in the samples. The doped sample shows improved visible light response than the pure α-Fe_2O_3 sample. The photocatalytic activity of the un-doped and doped sample was evaluated for the degradation of Rhodamine B dye under natural sunlight. A maximum degradation efficiency of 95% was obtained after a reaction time of 4 h [47]. Almazroai and co-workers prepared S-doped α-Fe_2O_3 nanomaterial by microwave irradiation (300 W for 20 min) using thiourea as sulphur precursor. The crystallinity of the α-Fe_2O_3 nanomaterial has found to decrease after S doping on the α-Fe_2O_3 lattice. After the sulphur-doping enhancement in the visible light absorption, intensity was noticed with a small decrease in the band gap value. This enhancement in the absorbance intensity of the doped photocatalyst can be attributed to the charge transition between the p-orbitals of the S atom and the conduction band (CB) of the α-Fe_2O_3 nanomaterial. The S-doped α-Fe_2O_3 nanomaterial display improved photocatalytic degradation efficiency than the pristine α-Fe_2O_3 nanomaterial [48]. Suganthi and co-workers fabricated metal (M = Cu, Ni and Co)-doped iron oxide (α-Fe_2O_3) nanoparticle by chemical precipitation followed by calcination. The specific surface area and mesoporosity of the Fe_2O_3 increases after doping with metal was observed. The metal-doped α-Fe_2O_3 exhibits higher photocatalytic activity than the pristine α-Fe_2O_3 nanomaterial towards the degradation of Acid Red-27 organic dye under visible light illumination. Among the metal-doped α-Fe_2O_3 materials, the Cu-doped α-Fe_2O_3 exhibits highest photocatalytic activity [49]. Gao and co-workers prepared multiple metal-doped Fe_3O_4@Fe_2O_3 nanoparticles from Waelz slag, an iron containing hazardous waste. They have employed acidolysis, sol–gel and calcination in order to prepare the multiple metal (Al, Zn, Cu and Mn)-doped Fe_3O_4@Fe_2O_3 nanoparticles from the waste slog. The photocatalytic activities of the synthesized multiple-metal-doped Fe_3O_4@Fe_2O_3 nanoparticles as well as the pristine Fe_2O_3 nanoparticles were compared for the photocatalytic degradation of methyl orange dye under UV and simulated sun light irradiation. It was observed that all of the doped Fe_3O_4@Fe_2O_3 nanoparticles shows improved photocatalytic activities as compared

to the pristine Fe_2O_3 [50]. So far, TiO_2 and ZnO are widely studied UV-active photocatalyst. However, there UV light response and poor separation of charge carriers limits their practical utility. Hence, a lot of research effort has been made in recent past in order to make heterojunction and composite by combining with different suitable visible light active semiconductor photocatalyst. α-Fe_2O_3 is a narrow band gap visible light active photocatalyst and its suitable band alignment makes α-Fe_2O_3 an ideal candidate to combine with other wide band gap semiconductor with improved light absorption and charge carrier separation ability. In the subsequent text, we will discuss the research progress in the preparation of composite/heterojunction of α-Fe_2O_3 with various semiconducting photocatalytic materials.

Omri and co-workers recently fabricated α-Fe_2O_3/TiO_2 nanocomposite material containing 10 and 50 mol% of TiO_2 by using a simple precipitation method. The α-Fe_2O_3/TiO_2 nanocomposite materials were characterized using various analytical instruments and studied as photocatalyst to degrade methylene blue dye (MB) under visible light. A maximum of 92% of MB dye degradation was recorded after 120 min of irradiation by using α-Fe_2O_3/TiO_2 composite material 50 mol% of TiO_2, whereas the pure α-Fe_2O_3 and TiO_2 exhibited relatively lower photocatalytic efficiency than the composite materials. Under the visible light, the TiO_2 material is unable to generate electron–hole pair, whereas the α-Fe_2O_3 material produce electron–hole pair. After material contact, the excited electron from the conduction band (CB) of α-Fe_2O_3 migrate to the CB of TiO_2, whereas the hole accumulate in the valance band (VB). This process minimize the recombination process of photogenerated electron–hole pair. The improved visible light absorption and charge carrier separation properties are account for the higher photocatalytic activity of the α-Fe_2O_3/TiO_2 nanocomposite material [51]. Qu and co-workers prepared α-Fe_2O_3/TiO_2 dendritic heterostructure nanomaterials in a two-step processes, first TiO_2 nanofiber prepared by electrospinning method and in second step the α-Fe_2O_3 nanomaterial deposited over the TiO_2 nanofiber by hydrothermal method. Four different sets of α-Fe_2O_3/TiO_2 dendritic heterostructure materials were prepared containing different amount of α-Fe_2O_3. From morphology, it is clearly seen that the heterostructure are comprises of TiO_2 nanofiber (diameter 70 nm) and α-Fe_2O_3 nanorods (length 100–200 nm and diameter ~ 30 nm), and the TiO_2 nanofibers are homogeneously covered by the α-Fe_2O_3 nanorods giving a typical branched and dendritic heterostructure configuration. The heterostructure materials exhibit enhanced visible light absorption feature. The photocatalytic activity of the α-Fe_2O_3/TiO_2 dendritic heterostructure nanomaterials demonstrated towards the degradation of a wide range of organic dye pollutants such as Congo red (CR), methylene blue (MB), methyl orange (MO) and eosin red (ER). All the heterostructure materials show enhanced degradation efficiency than the parent TiO_2 and commercial α-Fe_2O_3 materials. The enhanced photocatalytic activity of the heterostructured material is due to improved visible light response, charge carrier separation and efficient generation of hydroxyl radical [52]. Fu and co-workers fabricated magnetic γ-Fe_2O_3 nanosheets/mesoporous black TiO_2 hollow spherical heterojunctions material by employing a metal-ion intervened hydrothermal process followed by high-temperature hydrogenation technique. The hybrid γ-Fe_2O_3/b-TiO_2 hollow structure material have high specific surface area of $\sim 63\ m^2/g$ and a pore size

of 10.5 nm. The resulting hybrid material contains oxygen vacancies which influence the recombination process of electron–hole pairs and extend the lifetime of the charge carriers, by this means improving the photocatalytic performance of the photocatalyst. The photocatalytic activity of the hybrid γ-Fe_2O_3/b-TiO_2 heterojunctions material has been studied by degrading tetracycline pollutant. The hybrid γ-Fe_2O_3/b-TiO_2 display the photocatalytic degradation efficiency about three times greater than that of the pristine photocatalyst. The high photocatalytic property of hybrid γ-Fe_2O_3/b-TiO_2 heterojunctions is account to the narrow bandgap nature which extending the photo response from visible light to near infrared regions and the efficient separation and trapping of charge carrier due to generation of vacancies [53]. Jeevanandam and co-workers have synthesized TiO_2@α-Fe_2O_3 core–shell nanoheterostructured material by using a simple thermal decomposition technique. Microscopic studies confirm the deposition of the uniform α-Fe_2O_3 shell on the surface of TiO_2 spheres. The photocatalytic application of the TiO_2@α-Fe_2O_3 core–shell nanoheterostructured material was explored towards the degradation of RhB dye under sunlight illumination. The nanoheterostructured material displays enhanced photocatalytic ability than the pristine TiO_2 and α-Fe_2O_3 materials. This enhanced photocatalytic activity of the heterostructured material can be ascribed to the facile transfer of electrons from TiO_2 and α-Fe_2O_3 phase, which reduce the recombination processes of electron–hole pair over the photocatalyst surface [54].

The zinc oxide (ZnO) is an n-type wide band gap semiconductor, low price and non-toxic nature and a very good photocatalyst photocatalysis. Zhang and co-workers fabricate of magnetic 3D γ-Fe_2O_3@ZnO core–shell nanomaterial by using hydrothermal sintering followed by atomic layer deposition (ALD) method. ZnO shell layer was uniformly deposited on the γ-Fe_2O_3 core. The band alignment of the γ-Fe_2O_3 and ZnO photocatalyst are so aligned in a manner to give the characteristic feature of a type-II heterojunction photocatalyst. The photocatalytic activity of the synthesized core–shell nanomaterial was evaluated for ciprofloxacin degradation under simulated sun light illumination. The hydroxyl radical and the hole contribute significantly on the degradation of ciprofloxacin is noticed. The γ-Fe_2O_3@ZnO core–shell nanomaterial displays enhanced photocatalytic efficiency than the pristine γ-Fe_2O_3 and ZnO counterpart. The improved photocatalytic activity of the heterostructured material is due to the formation of type-II heterojunction and the core–shell structure, which facilitate the efficient migration and separation of the charge carrier [55]. Carmalt and co-workers fabricate α-Fe_2O_3/ZnO heterojunction films by using aerosol-assisted chemical vapour deposition technique. The band alignment and electron migration gives a characteristic feature of a type-I heterojunction system. The prepared α-Fe_2O_3/ZnO heterojunction films exhibit remarkably improved photocatalytic efficiency towards the degradation of stearic acid under UVA light, which is 16 times higher than that of the α-Fe_2O_3 and 2.5 times than that of the ZnO photocatalysts. Upon irradiation photogenerated electrons migrate from the CB of ZnO layer to the α-Fe_2O_3 layer that increase the life time of the electron which is responsible for the enhanced photocatalytic property of the α-Fe_2O_3/ZnO heterojunction films [56]. Mohapatra and co-workers fabricated a ternary α-Fe_2O_3/$ZnFe_2O_4$/

ZnO nanohybrid material by using a microwave-assisted co-precipitation and co-precipitation and thermal annealing synthesis technique. The co-precipitation method gives raise to nanoparticle where microwave-assisted synthesis gives nanodisks like morphology of the ternary photocatalyst. The ternary α-Fe_2O_3/$ZnFe_2O_4$/ZnO photocatalyst materials were examined as photocatalyst towards the degradation of methylene blue and malachite green dyes under solar light. The material prepared by using microwave-assisted synthesis shows highest photocatalytic activity than the material obtained by co-precipitation method. A maximum of 93.2% of MB degradation noticed after 32 min of irradiation using the α-Fe_2O_3/$ZnFe_2O_4$/ZnO nanodisks. The hydroxyl radical plays a crucial role in the degradation of the organic dyes which was confirmed from the radical scavenger experiment. They have proposed a cascade movement of electron across the CB band of the three component of the ternary photocatalyst, which efficiently reduce the recombination rate of the photogenerated charge carriers. This property may accountable for the improved photocatalytic activity of the synthesized ternary photocatalytic material [57]. Hota and co-workers have fabricated Fe_2O_3/$ZnFe_2O_4$, $ZnFe_2O_4$/ZnO and Fe_2O_3/$ZnFe_2O_4$/ZnO binary and ternary composite photocatalyst systems by using a simple hydrothermal method followed by calcination at 500 °C. All the synthesized nanocomposite materials display improved visible response as compared to the Fe_2O_3 material. The Fe_2O_3/$ZnFe_2O_4$/ZnO ternary composite material has the highest specific surface area of 49.464 m^2/g, which is much higher than that of the pure Fe_2O_3 and the binary composite material. The photocatalytic activity of the synthesized composite materials was evaluated for the degradation of malachite green (MG) dye under natural sunlight. A maximum of 96.92% of degradation of MG dye was achieved after 90 min of irradiation using the Fe_2O_3/$ZnFe_2O_4$/ZnO ternary composite material. They have proposed a cascade migration of electron across the CB of the different component of the ternary photocatalyst, which significantly reduce the recombination process of charge carriers [58].

Graphic carbon nitride (g-C_3N_4) has been emerged as a potential visible light active photocatalyst with a band gap of 2.7 eV due to high chemical stability, suitable band alignment, natural abundance and easy synthesis. However, low specific surface area, moderate band gap value and poor separation of photogenerated charge carriers limits its practical applications. So many research approaches have been made in recent past in order to prepare composite and heterojunction with Fe_2O_3, which has a suitable band alignment to prepare hybrid material with improved visible light response and charge carrier separation properties. Lu and co-workers has recently fabricated a series of α-Fe_2O_3/g-C_3N_4 hybrid materials and studied their photocatalytic activity towards tetracycline degradation under visible light. The α-Fe_2O_3/g-C_3N_4 hybrid materials were prepared by the calcination of Fe-based metal organic framework (Fe-MOF) and melamine. They have demonstrated the uniform distribution of α-Fe_2O_3 nanoparticles (3–5 nm) over the porous g-C_3N_4 nanosheet. The existence of close microscopic contact between these two phases further confirmed

from the TEM analysis. The α-Fe_2O_3/g-C_3N_4 hybrid material displays higher photocatalytic activity than the bulk g-C_3N_4 photocatalyst. The band alignment of both the component of the hybrid α-Fe_2O_3/g-C_3N_4 material are aligned in a type-II fashion, and this is responsible for the enhanced charge carrier separation and photocurrent density. The improved visible light absorption, greater specific surface area and efficient charge carrier separation property of the α-Fe_2O_3/g-C_3N_4 hybrid material are responsible for the enhanced photocatalytic activity [59]. Prakasam and co-workers prepared g-C_3N_4/α-Fe_2O_3 hybrid nanocomposites material by changing the mass ratio of both the components by using a simple one-step hydrothermal method. The photocatalytic activity of the hybrid material evaluated by degrading Congo red (CR) and malachite green (MG) dye under visible light. The FESEM study of g-C_3N_4/α-Fe_2O_3 composite material clearly indicates the incorporation of α-Fe_2O_3 nanoparticles over the g-C_3N_4 nanosheet. The absorption edge of both the pristine g-C_3N_4 and α-Fe_2O_3 materials commence around 455 and 460 nm, respectively. A considerable red shift in the absorption edge was observed for the hybrid material indicating the better visible light absorption and decrease in the band gap value of the photocatalyst. The hybrid material exhibits 87 and 95% of CR and MG dyes degradation after 100 min of irradiation time, which is around 2 times higher than that of the pristine g-C_3N_4 photocatalyst. The type-II nature of the electron–hole migration in the heterojunction is responsible for the higher photocatalytic activity of the hybrid photocatalyst [60]. Li and co-workers prepared a cocoon-shaped magnetic Fe_2O_3/g-C_3N_4 nanocomposite material by two-step hydrothermal synthesis. The cocoon-shaped Fe_2O_3 dispersed uniformly over the porous and layered g-C_3N_4 surface. The Fe_2O_3/g-C_3N_4 composite photocatalyst exhibits better photocatalytic efficiency for the degradation of Rhodamine B dye than the pristine Fe_2O_3 and g-C_3N_4 counterpart [61]. Li and co-workers prepared a Z-scheme g-C_3N_4/α-Fe_2O_3 heterojunction photocatalytic system with enhanced charge carrier separation and photocatalytic activity. They have demonstrated the establishment of the Fe–O–C bond in the heterojunction system, which believe to induce facile migration of electron across the grain boundary. The improved visible light response and facile migration of electron makes the heterojunction photocatalyst a better one than the pristine counterpart towards visible light-induced degradation of methylene blue dye [62]. Due to narrow band gap nature and suitable band alignment of the Fe_2O_3 semiconducting nanoparticle, it is not only involve in making hybrid photocatalyst with TiO_2, ZnO and g-C_3N_4 but also a lot of new Fe_2O_3-based hybrid materials with improved photocatalytic activity that has been evolved with time. The Fe_2O_3-based hybrid materials, their synthesis method, photocatalytic application and their photocatalytic efficiency is presented in Table 4.1.

Table 4.1 Photocatalytic applications of different Fe_2O_3-based photocatalyst

Materials	Methods	Photocatalytic application	Photocatalytic performance	References
TiO_2/Fe_2O_3/CNTs	Sol–gel and calcination	Tetracycline degradation	89.41% in 90 min	[63]
$SiO_2/TiO_2/Fe_2O_3$	Mechanochemical	Methylene blue degradation	97% in 22 h	[64]
$Ag_3PO_4–TiO_2–Fe_2O_3$	Solid state blending	Orange II	86.71% in 30 min	[65]
Fe_2O_3/g-C_3N_4@N-TiO_2	Electrochemical anodization, calcination	Bisphenol-A degradation	100% in 80 min	[66]
Fe_2O_3 @SiO_2 @TiO_2	Solvothermal, layer-by-layer assembly	Phenol degradation	100% in 1 h	[67]
α-Fe_2O_3@TiO_2 core–shell	Hydrothermal synthesis	Acid orange 7 degradation	98.6% in 90 min	[68]
$Fe_2O_3–TiO_2$	Template-assisted dipping/ adsorbing-calcining strategy	Methyl blue degradation	95% in 25 min	[69]
g-C_3N_4/γ-Fe_2O_3/TiO_2	Sol–gel	Cefixime trihydrate degradation	98.09% in 90 min	[70]
α-Fe_2O_3@TiO_2 core–shell	Hetero-epitaxial growth	Rhodamine B degradation	60% in 5 h	[71]
Fe_2O_3 @TiO_2@nanometal (Au, Ag)	Sol–gel	Methylene blue degradation	92% in 2 h	[72]
TiO_2/Au/Fe_2O_3	Metal-organic framework (MOF) route	2,4 dichlorophenol	94% in 90 min	[73]
TiO_2 and γ-Fe_2O_3@GO/PANI-NT	Co-precipitation, hydrolysis-calcination	Rhodamine B degradation	94% in 140 min	[74]
Carbon/TiO_2/Fe_2O_3	Hydrolysis and hydrothermal procedures	Methylene blue degradation	97% in 100 min	[75]
α-$Fe_2O_3–TiO_2$/fly ash	Sol–gel	Rhodamine B degradation	100% in 1 h	[76]
Fe_2O_3/TiO_2	Sol–gel	4-chlorophenol degradation	100% in 180 min	[77]
Fe_2O_3/ZnO/$ZnFe_2O_4$	Hydrothermal and annealing	Rhodamine B degradation	95.7% in 60 min	[78]
CuO/Fe_2O_3/ZnO	Sol–gel combustion	Bisphenol A degradation	97.5% in 180 min	[79]
Zeolite-supported ZnO/Fe_2O_3/MnO_2	One-step impregnation method	Methylene blue degradation	93% in 120 min	[80]

(continued)

Table 4.1 (continued)

Materials	Methods	Photocatalytic application	Photocatalytic performance	References
Fe_2O_3/ZnO	Solution-combustion technique	Rhodamine 6G degradation	100% in 4 h	[81]
Cu–Fe_2O_3/Ni–ZnO	Hydrothermal, precipitation and calcination	Tetracycline degradation	94% in 2 h	[82]
γ-Fe_2O_3/g-C_3N_4	Thermal heating and hydrothermal treatment	Tetracycline degradation	73.8% in 120 min	[83]
g-C_3N_4–Fe_2O_3	Calcination	Methyl orange degradation	99% in 120 min	[84]
$BaTiO_3$/α-Fe_2O_3	Thermal annealing	Rhodamine B degradation	> 95% in 120 min	[85]
$KNbO_3$/α-Fe_2O_3	Hydrothermal method	Methylene blue degradation	89% in 90 min	[86]
α-Fe_2O_3/RGO	Hydrothermal method	Phenol degradation	62% in 150 min	[87]
α-Fe_2O_3/CdS	Wet-chemical method	Methylene blue degradation	86.7% in 120 min	[88]
SnO_2/α-Fe_2O_3	Chemical vapour deposition	Methylene blue degradation	100% in 2.5 h	[89]
SnO_2/α-Fe_2O_3–PB (Prussian blue) thin films	Electrochemical and annealing	Rhodamine B and Congo red degradation	~ 80% CR and ~ 82% RhB in 120 min	[90]
α-Fe_2O_3/Ag/AgX (X = Cl, Br, I)	In-situ oxidation reaction and self-assembly process	Rhodamine B degradation	100% in 60 min	[91]
α-Fe_2O_3/rGO	Hydrothermal method	Rhodamine 6G degradation	90.5% in 4 h	[92]
$CaFe_2O_4$/Fe_2O_3	Hydrothermal and co-precipitation method	Methyl orange degradation	99% in 60 min	[93]
NiO–Fe_2O_3–CdO	Precipitation and calcination	Methyl orange degradation	84.25% in 60 min	[94]
ZnS/Fe_2O_3/Ag	Hydrothermal method	Eosin blue degradation	93% in 60 min	[95]
Fe_2O_3/Mn_2O_3	Sol–gel method	Parathion degradation	90% in 15 min	[96]
α-Fe_2O_3@rGO/PAN	Hydrothermal method	Methylene blue degradation	98.5% in 2 h	[97]
Ag/AgBr@Fe_2O_3	Solvothermal method	Methyl orange degradation	94.4% in 12 min	[98]

(continued)

Table 4.1 (continued)

Materials	Methods	Photocatalytic application	Photocatalytic performance	References
$SrTiO_3/Fe_2O_3$	Hydrothermal and electrospinning technique	Tetracycline degradation	82.7% in 140 min	[99]
$Ag_3PO_4/\alpha\text{-}Fe_2O_3$	Hydrothermal method	Rhodamine B degradation	95% in 10 min	[100]
Fe_2O_3/Cu_2O	Hydrothermal method	Rhodamine B degradation	91.25% in 120 min	[101]
$Fe_2O_3@WO_3$	Hydrothermal method and precipitation	Rhodamine B degradation	98% in 75 min	[102]
$\alpha\text{-}Fe_2O_3/Ag_6Si_2O_7$	Wet chemical method	Methylene blue degradation	98% in 30 min	[103]
$Fe_2O_3/CuBi_2O_4$	Hydrothermal method	Tetracycline degradation	80% in 120 min	[104]
Fe_2O_3/Ag_3VO_4	Solvothermal and precipitation method	Rhodamine B degradation	96.1% in 60 min	[105]
CeO_2/Fe_2O_3	Co-precipitation method	Eosin yellow degradation	98% in 25 min	[106]
Fe_2O_3/BiOCl	Hydrothermal method	Methyl orange-Rhodamine B mixed dye degradation	90% in 30 min	[107]
$CuO/\alpha\text{-}Fe_2O_3/\gamma\text{-}Al_2O_3$	Precipitation method	Methyl orange degradation	98% in 240 min	[108]
$SnO_2–Fe_2O_3–rGO$	Hydrothermal method	Crystal violet degradation	96.3% in 120 min	[109]
$\alpha\text{-}Fe_2O_3/BiVO_4$	Hydrothermal method	Tetracycline degradation	> 80% in 120 min	[110]
$Fe_2TiO_5/\alpha\text{-}Fe_2O_3/TiO_2$	Combustion synthesis	Methylene blue degradation	> 95% in 120 min	[16]
$\alpha\text{-}Fe_2O_3/BiFeO_3$	Hydrothermal method	Rhodamine B degradation	60% in 4 h	[111]
$FeWO_4/Fe_2O_3$ di-modified WO_3	Hydrothermal method	Methylene blue degradation	95% in 10 min	[112]
$\gamma\text{-}Fe_2O_3@SiO_2@AgBr$:Ag	Solvothermal, Stöber method	Acid orange 7 degradation	> 90% in 20 min	[113]
$\alpha\text{-}Fe_2O_3$-doped Ti_3C_2 MXene	Ultrasonic assisted self-assembly method	Rhodamine B degradation	98% in 120 min	[114]
$\alpha\text{-}Fe_2O_3$@UiO-66	Wet chemical method and calcination	Methylene blue degradation	> 95% in 60 min	[115]
Fe_2O_3/Bi_2S_3	Hydrothermal method	Methylene blue degradation	~ 90% in 5 h	[116]

(continued)

Table 4.1 (continued)

Materials	Methods	Photocatalytic application	Photocatalytic performance	References
γ-Fe_2O_3/BiOI	Sol–gel, microwave hydrothermal method	Methyl orange degradation	86.3% in 120 min	[117]
Ag_2CO_3/α-Fe_2O_3	Precipitation and hydrothermal method	Malachite green degradation	~ 90% in 120 min	[118]
ZnS/Fe_2O_3	Hydrothermal method	Methylene blue degradation	90.17% in 4 h	[119]
C_3N_4@$CoFe_2O_4$/Fe_2O_3	Hydrothermal and calcination method	Tetracycline degradation	99.7% in 80 min	[120]
P3HT/α-Fe_2O_3	Electrophoretic deposition	Tetracycline degradation	97% in 90 min	[121]

4.4 Conclusions

In this chapter, we emphasized the photocatalytic applications of iron oxide and iron oxide-based materials towards the degradation of various persistent aqueous organic pollutants such as dyes, pesticides and phenolic compounds. In terms of synthesis, this chapter provides an overview of morphology control preparation of phase pure iron oxide as well as single-step and multiple-step preparation of iron oxide-based hybrid materials. We believe that this chapter gives an idea in order to prepare iron oxide-based hybrid materials and their applications in the emerging field of research such as electronic, energy and environment.

Acknowledgements The authors are thankful to Prof. Braja Gopal Mishra, Dr. Dibyananda Majhi and Krishnendu Das, Department of Chemistry, National Institute of Technology Rourkela, Odisha, India, for their timely help and valuable discussions.

References

1. Zou LY, Li Y, Hung YT (2007) Wet air oxidation for waste treatment. In: Wang LK, Hung YT, Sharma NK (eds) Advanced physicochemical treatment technologies. Handbook of environmental engineering, vol 5. Humana Press. https://doi.org/10.1007/978-1-59745-173-4_13
2. Saxena R, Saxena M, Lochab A (2020) Recent progress in nanomaterials for adsorptive removal of organic contaminants from wastewater. ChemistrySelect 5:335–353. https://doi.org/10.1002/slct.201903542
3. Jain M, Khan AS, Sharm K, Jadhao PR, Pant KK, Ziora ZM, Blaskovich MAT (2022) Current perspective of innovative strategies for bioremediation of organic pollutants from wastewater. Bioresour Technol 344:126305. https://doi.org/10.1016/j.biortech.2021.126305
4. Nakata K, Fujishima A (2012) TiO_2 photocatalysis: design and applications. J Photochem Photobiol C Photochem Rev 13:169–189. https://doi.org/10.1016/j.jphotochemrev.2012.06.001
5. Hitam CNC, Jalil AA (2020) A review on exploration of Fe_2O_3 photocatalyst towards degradation of dyes and organic contaminants. J Environ Manage 258:110050. https://doi.org/10.1016/j.jenvman.2019.110050
6. Wu W, Jiang C, Roy VAL (2015) Recent progress in magnetic iron oxide–semiconductor composite nanomaterials as promising photocatalysts. Nanoscale 7:38–58. https://doi.org/10.1039/C4NR04244A
7. Lai MTL, Lee KM, Yang TCK, Pan GT, Lai CW, Chen CY, Johan MR, Juan JC (2021) The improved photocatalytic activity of highly expanded MoS_2 under visible light emitting diodes. Nanoscale Adv 3:1106. https://doi.org/10.1039/D0NA00936A
8. Cheng L, Xiang Q, Liao Y, Zhang H (2018) CdS-based photocatalysts. Energy Environ Sci 11:1362–1391. https://doi.org/10.1039/C7EE03640J
9. Mishra M, Chun DM (2015) α-Fe_2O_3 as a photocatalytic material: a review. Appl Catal A 498:126–141. https://doi.org/10.1016/j.apcata.2015.03.023
10. Bhoi YP, Rout DP, Mishra BG (2016) Photocatalytic chemoselective aerobic oxidation of thiols to disulfides catalyzed by combustion synthesized bismuth tungstate nanoparticles in aqueous media. J Clust Sci 27:267–284. https://doi.org/10.1007/s10876-015-0928-0

11. Bhoi YP, Mishra BG (2018) Synthesis, characterization, and photocatalytic application of type-II CdS/$Bi_2W_2O_9$ heterojunction nanomaterials towards aerobic oxidation of amines to imines. Eur J Inorg Chem 2648–2658. https://doi.org/10.1002/ejic.201800221
12. Bhoi YP, Mishra BG (2018) Photocatalytic degradation of alachlor using type-II CuS/$BiFeO_3$ heterojunctions as novel photocatalyst under visible light irradiation. Chem Eng J 344:391–401. https://doi.org/10.1016/j.cej.2018.03.094
13. Yang Y, Zhang C, Lai C, Zeng G, Huang D, Cheng M, Wang J, Chen F, Zhou C, Xiong W (2018) BiOX (X = Cl, Br, I) photocatalytic nanomaterials: applications for fuels and environmental management. Adv Colloid Interface Sci 254:76–93. https://doi.org/10.1016/j.cis.2018.03.004
14. Marschall R (2014) Semiconductor composites: strategies for enhancing charge carrier separation to improve photocatalytic activity. Adv Funct Mater 24:2421–2440. https://doi.org/10.1002/adfm.201303214
15. Wang Y, Wang Q, Zhan X, Wang F, Safdar M, He J (2013) Visible light driven type II heterostructures and their enhanced photocatalysis properties: a review. Nanoscale 5:8326–8339. https://doi.org/10.1039/C3NR01577G
16. Bhoi YP, Fang F, Zhou X, Li Y, Sun X, Wang J, Huang W (2020) Single step combustion synthesis of novel Fe_2TiO_5/α-Fe_2O_3/TiO_2 ternary photocatalyst with combined double type-II cascade charge migration processes and efficient photocatalytic activity. Appl Surf Sci 525:146571. https://doi.org/10.1016/j.apsusc.2020.146571
17. Majhi D, Samal PK, Das K, Gouda SK, Bhoi YP, Mishra BG (2019) α-NiS/Bi_2O_3 nanocomposites for enhanced photocatalytic degradation of tramadol. ACS Appl Nano Mater 2(1):395–407. https://doi.org/10.1021/acsanm.8b01974
18. Majhi D, Bhoi YP, Samal PK, Mishra BG (2018) Morphology controlled synthesis and photocatalytic study of novel CuS-$Bi_2O_2CO_3$ heterojunction system for chlorpyrifos degradation under visible light illumination. Appl Surf Sci 455:891–902. https://doi.org/10.1016/j.apsusc.2018.06.051
19. Bhoi YP, Majhi D, Das K, Mishra BG (2019) Visible-light-assisted photocatalytic degradation of phenolic compounds using Bi_2S_3/$Bi_2W_2O_9$ heterostructure materials as photocatalyst. ChemistrySelect 4(12):3423–3431. https://doi.org/10.1002/slct.201900450
20. Majhi D, Das K, Bariki R, Padhan S, Mishra A, Dhiman R, Dash P, Nayak B, Mishra BG (2020) A facile reflux method for in situ fabrication of a non-cytotoxic Bi_2S_3/β-Bi_2O_3/$ZnIn_2S_4$ ternary photocatalyst: a novel dual Z-scheme system with enhanced multifunctional photocatalytic activity. J Mater Chem A 8:21729–21743. https://doi.org/10.1039/D0TA06129H
21. Das K, Majhi D, Bhoi YP, Mishra BG (2019) Combustion synthesis, characterization and photocatalytic application of CuS/$Bi_4Ti_3O_{12}$ p–n heterojunction materials towards efficient degradation of 2-methyl-4-chlorophenoxyacetic acid herbicide under visible light. Chem Eng J 362:588–599. https://doi.org/10.1016/j.cej.2019.01.060
22. Bhoi YP, Behera C, Majhi D, Equeenuddin SM, Mishra BG (2018) Visible light-assisted photocatalytic mineralization of diuron pesticide using novel type II CuS/$Bi_2W_2O_9$ heterojunctions with a hierarchical microspherical structure. New J Chem 42:281–292. https://doi.org/10.1039/C7NJ03390G
23. Majhi D, Mishra AK, Das K, Bariki R, Mishra BG (2021) Plasmonic Ag nanoparticle decorated Bi_2O_3/$CuBi_2O_4$ photocatalyst for expeditious degradation of 17α-ethinylestradiol and Cr(VI) reduction: insight into electron transfer mechanism and enhanced photocatalytic activity. Chem Eng J 413:127506. https://doi.org/10.1016/j.cej.2020.127506
24. Bariki R, Majhi D, Das K, Behera A, Mishra BG (2020) Facile synthesis and photocatalytic efficacy of UiO-66/$CdIn_2S_4$ nanocomposites with flowerlike 3D-microspheres towards aqueous phase decontamination of triclosan and H_2 evolution. Appl Catal B 270:118882. https://doi.org/10.1016/j.apcatb.2020.118882
25. Das K, Majhi D, Bariki R, Mishra BG (2020) SnS_2/$Bi_4Ti_3O_{12}$ heterostructure material: a UV-visible light active direct Z-scheme photocatalyst for aqueous phase degradation of diazinon. ChemistrySelect 5(4):1567–1577. https://doi.org/10.1002/slct.201904532

26. Majhi D, Das K, Mishra A, Dhiman R, Mishra BG (2020) One pot synthesis of CdS/BiOBr/$Bi_2O_2CO_3$: a novel ternary double Z-scheme heterostructure photocatalyst for efficient degradation of atrazine. Appl Catal B 260:118222. https://doi.org/10.1016/j.apcatb.2019.118222
27. Das K, Bariki R, Majhi D, Mishra A, Das KK, Dhiman R, Mishra BG (2022) Facile synthesis and application of CdS/$Bi_{20}TiO_{32}$/$Bi_4Ti_3O_{12}$ ternary heterostructure: a synergistic multi-heterojunction photocatalyst for enhanced endosulfan degradation and hydrogen evolution reaction. Appl Catal B 303:120902. https://doi.org/10.1016/j.apcatb.2021.120902
28. Kharisov BI, Dias HVR, Kharissova OV, Perez VMJ, Pereza BO, Flores BM (2012) Iron-containing nanomaterials: synthesis, properties, and environmental applications. RSC Adv 2:9325–9358. https://doi.org/10.1039/C2RA20812A
29. Qu J, Yu Y, Cao CY, Song WG (2013) α-Fe_2O_3 nanodisks: layered structure, growth mechanism, and enhanced photocatalytic property. Chem Eur J 19:11172–11177. https://doi.org/10.1002/chem.201301295
30. Ghasemifard M, Heidari G, Ghamari M, Fathi E, Izi M (2019) Synthesis of porous network-like α-Fe_2O_3 and α/γ-Fe_2O_3 nanoparticles and investigation of their photocatalytic properties. Nanotechnol Russ 14:353–361. https://doi.org/10.1134/S1995078019040062
31. Sun W, Meng Q, Jing L, Liu D, Cao Y (2013) Facile synthesis of surface-modified nanosized α-Fe_2O_3 as efficient visible photocatalysts and mechanism insight. J Phys Chem C 117:1358–1365. https://doi.org/10.1021/jp309599d
32. Basnet P, Larsen GK, Jadeja RP, Hung YC, Zhao Y (2013) α-Fe_2O_3 nanocolumns and nanorods fabricated by electron beam evaporation for visible light photocatalytic and antimicrobial applications. ACS Appl Mater Interfaces 5:2085–2095. https://doi.org/10.1021/am303017c
33. Kormann C, Bahnemann DW, Hoffmann MR (1989) Environmental photochemistry: is iron oxide (hematite) an active photocatalyst? A comparative study: α-Fe_2O_3, ZnO, TiO_2. J Photochem Photobiol A Chem 48(1):161–169. https://doi.org/10.1016/1010-6030(89)87099-6
34. Aslam M, Qamar MT, Rehman AU, Soomro MT, Ali S, Ismail IMI, Hameed A (2018) The evaluation of the photocatalytic activity of magnetic and nonmagnetic polymorphs of Fe_2O_3 in natural sunlight exposure: a comparison of photocatalytic activity. Appl Surf Sci 451:128–140. https://doi.org/10.1016/j.apsusc.2018.04.219
35. Wang C, Zhu C, Ren X, Shi J, Wang L, Lv B (2019) Anisotropic photogenerated charge separations between different facets of a dodecahedral α-Fe_2O_3 photocatalyst. CrystEngComm 21:6390–6395. https://doi.org/10.1039/C9CE01143A
36. Sundaramurthy J, Kumar PS, Kalaivani M, Thavasi V, Mhaisalkara SG, Ramakrishna S (2012) Superior photocatalytic behaviour of novel 1D nanobraid and nanoporous α-Fe_2O_3 structures. RSC Adv 2:8201–8208. https://doi.org/10.1039/c2ra20608k
37. Xie S, Jia H, Lu F, Sun N, Yu J, Liu S, Zheng L (2015) Controlled synthesis of α-Fe_2O_3 nanostructures with the assistance of ionic liquid and their distinct photocatalytic performance under visible-light irradiation. CrystEngComm 17:1210–1218. https://doi.org/10.1039/c4ce02033b
38. Wang FL, Song X, Teng Y, Xia J, Xu ZY, Wang WP (2019) Synthesis, structure, magnetism and photocatalysis of α-Fe_2O_3 nanosnowflakes. RSC Adv 9:35372–35383. https://doi.org/10.1039/c9ra07490b
39. Liu X, Chen K, Shim JJ, Huang J (2015) Facile synthesis of porous Fe_2O_3 nanorods and their photocatalytic properties. J Saudi Chem Soc 19(5):479–484. https://doi.org/10.1016/j.jscs.2015.06.009
40. Liang C, Liu H, Zhou J, Peng X, Zhang H (2015) One-step synthesis of spherical γ-Fe_2O_3 nanopowders and the evaluation of their photocatalytic activity for Orange I degradation. J Chem 8. Article ID 791829. https://doi.org/10.1155/2015/791829
41. Fardood ST, Moradnia F, Moradi S, Forootan R, Zare FY, Heidari M (2019) Eco-friendly synthesis and characterization of α-Fe_2O_3 nanoparticles and study of their photocatalytic activity for degradation of Congo red dye. Nanochem Res 4(2):140–147. https://doi.org/10.22036/ncr.2019.02.005

42. Yin H, Zhao Y, Hua Q, Zhang J, Zhang Y, Xu X, Long Y, Tang J, Wang F (2019) Controlled synthesis of hollow α-Fe_2O_3 microspheres assembled with ionic liquid for enhanced visible-light photocatalytic activity. Front Chem 7:58. https://doi.org/10.3389/fchem.2019.00058
43. Xu JS, Zhu YJ (2011) α-Fe_2O_3 hierarchically hollow microspheres self-assembled with nanosheets: surfactant-free solvothermal synthesis, magnetic and photocatalytic properties. CrystEngComm 13:5162. https://doi.org/10.1039/c1ce05252g
44. Liu G, Deng Q, Wang H, Ng DHL, Kong M, Cai W, Wang G (2012) Micro/nanostructured α-Fe_2O_3 spheres: synthesis, characterization, and structurally enhanced visible-light photocatalytic activity. J Mater Chem 22:9704. https://doi.org/10.1039/c2jm31586f
45. Zhu LP, Bing NC, Wang LL, Jin HY, Liao GH, Wang LJ (2012) Self-assembled 3D porous flowerlike α-Fe_2O_3 hierarchical nanostructures: synthesis, growth mechanism, and their application in photocatalysis. Dalton Trans 41:2959. https://doi.org/10.1039/c2dt11822j
46. Geng B, Tao B, Li X, Wei W (2012) Ni^{2+}/surfactant-assisted route to porous α-Fe_2O_3 nanoarchitectures. Nanoscale 4:1671. https://doi.org/10.1039/c2nr12102f
47. Pradhan GK, Sahu N, Parida KM (2013) Fabrication of S, N co-doped α-Fe_2O_3 nanostructures: effect of doping, OH radical formation, surface area, [110] plane and particle size on the photocatalytic activity. RSC Adv 3:7912–7920. https://doi.org/10.1039/C3RA23088K
48. Almazroai LS, Maliabari LA (2020) Microwave synthesis of sulfur-doped α-Fe_2O_3 and testing in photodegradation of methyl orange. J Chin Chem Soc 67(10). https://doi.org/10.1002/jccs.202000035
49. Satheesh R, Vignesh K, Suganthi A, Rajarajan M (2014) Visible light responsive photocatalytic applications of transition metal (M = Cu, Ni and Co) doped α-Fe_2O_3 nanoparticles. J Environ Chem Eng 2:1956–1968. https://doi.org/10.1016/j.jece.2014.08.016
50. Li N, He Y, Yi Z, Gao L, Zhai F, Chattopadhyay K (2020) Multiple-metal-doped Fe_3O_4@Fe_2O_3 nanoparticles with enhanced photocatalytic performance for methyl orange degradation under UV/solar light irradiation. Ceram Int 46:19038–19045. https://doi.org/10.1016/j.ceramint.2020.04.234
51. Mansour H, Omri K, Bargougui R, Ammar S (2020) Novel α-Fe_2O_3/TiO_2 nanocomposites with enhanced photocatalytic activity. Appl Phys A 126:151. https://doi.org/10.1007/s00339-020-3320-3
52. Li X, Lin H, Chen X, Niu H, Liu J, Zhang T, Qu F (2016) Dendritic α-Fe_2O_3/TiO_2 nanocomposites with improved visible light photocatalytic activity. Phys Chem Chem Phys 18:9176–9185. https://doi.org/10.1039/c5cp06681f
53. Ren L, Zhou W, Sun B, Li H, Qiao P, Xu Y, Wu J, Lin K, Fu H (2019) Defects-engineering of magnetic γ-Fe_2O_3 ultrathin nanosheets/mesoporous black TiO_2 hollow sphere heterojunctions for efficient charge separation and the solar-driven photocatalytic mechanism of tetracycline degradation. Appl Catal B 240:319–328. https://doi.org/10.1016/j.apcatb.2018.08.033
54. Mahajan J, Jeevanandam P (2018) Synthesis of TiO_2@α-Fe_2O_3 core–shell heteronanostructures by thermal decomposition approach and their application towards sunlight driven photodegradation of Rhodamine B. New J Chem 42:2616–2626. https://doi.org/10.1039/c7nj04892k
55. Li N, Zhang J, Tian Y, Zhao J, Zhang J, Zuo W (2017) Precisely controlled fabrication of magnetic 3D γ-Fe_2O_3@ZnO core-shell photocatalyst with enhanced activity: ciprofloxacin degradation and mechanism insight. Chem Eng J 308:377–385. https://doi.org/10.1016/j.cej.2016.09.093
56. Jiamprasertboon A, Kafizas A, Sachs M, Ling M, Alotaibi AM, Lu Y, Siritanon T, Parkin IP, Carmalt CJ (2019) Heterojunction α-Fe_2O_3/ZnO films with enhanced photocatalytic properties grown by aerosol-assisted chemical vapour deposition. Chem Eur J 25(48):11337–11345. https://doi.org/10.1002/chem.201902175
57. Choudhary S, Bisht A, Mohapatra S (2021) Microwave-assisted synthesis of α-Fe_2O_3/$ZnFe_2O_4$/ZnO ternary hybrid nanostructures for photocatalytic applications. Ceram Int 47:3833–3841. https://doi.org/10.1016/j.ceramint.2020.09.243

58. Dhal JP, Mishra BG, Hota G (2015) Hydrothermal synthesis and enhanced photocatalytic activity of ternary $Fe_2O_3/ZnFe_2O_4/ZnO$ nanocomposite through cascade electron transfer. RSC Adv 5:58072. https://doi.org/10.1039/c5ra05894e
59. Wang B, Liu X, Dai S, Lu H (2020) α-Fe_2O_3 nanoparticles/porous g-C_3N_4 hybrids synthesized by calcinations of Fe-based MOF/melamine mixtures for boosting visible-light photocatalytic tetracycline degradation. ChemistrySelect 5:3303–3311. https://doi.org/10.1002/slct.201904388
60. Sumathi M, Prakasam A, Anbarasan PM (2019) A facile microwave stimulated g-C_3N_4/α-Fe_2O_3 hybrid photocatalyst with superior photocatalytic activity and attractive cycling stability. J Mater Sci Mater Electron 30:10985–10993. https://doi.org/10.1007/s10854-019-01439-1
61. Yu X, Yang X, Li G (2018) Magnetically separable Fe_2O_3/g-C_3N_4 nanocomposites with cocoon-like shape: magnetic properties and photocatalytic activities. J Electron Mater 47(1):672–676. https://doi.org/10.1007/s11664-017-5835-8
62. Yu Q, Yang K, Li H, Li X (2021) Z-scheme α-Fe_2O_3/g-C_3N_4 with the Fe–OC–bond toward enhanced photocatalytic degradation. Colloids Surf A Physicochem Eng Asp 616:126269. https://doi.org/10.1016/j.colsurfa.2021.126269
63. Lu C, Guan W, Zhang G, Ye L, Zhou Y, Zhang X (2013) TiO_2/Fe_2O_3/CNTs magnetic photocatalyst: a fast and convenient synthesis and visible-light-driven photocatalytic degradation of tetracycline. Micro Nano Lett 8(10):749–752. https://doi.org/10.1049/mnl.2013.0428
64. Kucio K, Charmas B, Pasieczna-Patkowska S, Zięzio M (2020) Mechanochemical synthesis of nanophotocatalysts $SiO_2/TiO_2/Fe_2O_3$: their structural, thermal and photocatalytic properties. Appl Nanosci 10:4733–4746. https://doi.org/10.1007/s13204-020-01462-3
65. Ana L, Meng Y, Wang T, Xiong C, Yan Z, Xu Z (2020) Highly efficient and easily recoverable Ag_3PO_4–TiO_2–Fe_2O_3 magnetic photocatalyst with wide spectral range for water treatment. Russ J Phys Chem A 94(5):1067–1072. https://doi.org/10.1134/S0036024420050027
66. Kong X, Lia J, Yang C, Tang Q, Wang D (2020) Fabrication of Fe_2O_3/g-C_3N_4@N-TiO_2 photocatalyst nanotube arrays that promote bisphenol A photodegradation under simulated sunlight irradiation. Sep Purif Technol 248:116924. https://doi.org/10.1016/j.seppur.2020.116924
67. Szeto W, Li J, Huang H, Xu J, Leung DYC (2015) Novel urchin-like Fe_2O_3@SiO_2@TiO_2 microparticles with magnetically separable and photocatalytic properties. RSC Adv 5:55363. https://doi.org/10.1039/c5ra08070c
68. Liu J, Yang S, Wu W, Tian Q, Cui S, Dai Z, Ren F, Xiao X, Jiang C (2015) 3D flowerlike α-Fe_2O_3@TiO_2 core–shell nanostructures: general synthesis and enhanced photocatalytic performance. ACS Sustain Chem Eng 3:2975–2984. https://doi.org/10.1021/acssuschemeng.5b00956
69. Luo H, Yu S, He F, Li L, Zhong M, Dong N, Su B (2021) An important phenomenon in Fe_2O_3–TiO_2 photocatalyst: ion-inter-doping. Solid State Sci 113:106538. https://doi.org/10.1016/j.solidstatesciences.2021.106538
70. Jahanshahi R, Sobhani S, Sansano JM (2020) High performance magnetically separable g-C_3N_4/γ-Fe_2O_3/TiO_2 nanocomposite with boosted photocatalytic capability towards the cefixime trihydrate degradation under visible-light. ChemistrySelect 5:10114–10127. https://doi.org/10.1002/slct.202002682
71. Xia Y, Yin L (2013) Core–shell structured α-Fe_2O_3@TiO_2 nanocomposites with improved photocatalytic activity in the visible light region. Phys Chem Chem Phys 15:18627–18634. https://doi.org/10.1039/c3cp53178c
72. Kim SE, Woo JY, Kang SY, Min BK, Lee JK, Lee SW (2016) A facile general route for ternary Fe_2O_3@TiO_2@nanometal (Au, Ag) composite as a high-performance and recyclable photocatalyst. J Ind Eng Chem 43:142–149. https://doi.org/10.1016/j.jiec.2016.07.060
73. Li Y, Yang B, Liu B (2021) MOF assisted synthesis of TiO_2/Au/Fe_2O_3 hybrids with enhanced photocatalytic hydrogen production and simultaneous removal of toxic phenolic compounds. J Mol Liq 322:114815. https://doi.org/10.1016/j.molliq.2020.114815

74. Ghavami M, Kassaee MZ, Mohammadi R, Koohi M, Haerizadeh BN (2014) Polyaniline nanotubes coated with TiO_2&γ-Fe_2O_3@graphene oxide as a novel and effective visible light photocatalyst for removal of Rhodamine B from water. Solid State Sci 38:143–149. https://doi.org/10.1016/j.solidstatesciences.2014.09.010
75. Wang M, Han J, Yuan G, Guo R (2019) Carbon/TiO_2/Fe_2O_3 hybrid shells toward efficient visible light photocatalysts. New J Chem 43:11282–11287. https://doi.org/10.1039/C9NJ01742A
76. Liu S, Zhu J, Guo X, Ge J, Wu H (2015) Preparation of α-Fe_2O_3–TiO_2/fly ash cenospheres photocatalyst and its mechanism of photocatalytic degradation. Colloids Surf A Physicochem Eng Asp 484:434–440. https://doi.org/10.1016/j.colsurfa.2015.08.033
77. Palanisamy B, Babu CM, Sundaravel B, Anandan S, Murugesan V (2013) Sol–gel synthesis of mesoporous mixed Fe_2O_3/TiO_2 photocatalyst: application for degradation of 4-chlorophenol. J Hazard Mater 252–253:233–242. https://doi.org/10.1016/j.jhazmat.2013.02.060
78. Li X, Jin B, Huang J, Zhang Q, Peng R, Chu S (2018) Fe_2O_3/ZnO/$ZnFe_2O_4$ composites for the efficient photocatalytic degradation of organic dyes under visible light. Solid State Sci 80:6–14. https://doi.org/10.1016/j.solidstatesciences.2018.03.016
79. Shekoohiyan S, Rahmani A, Chamack M, Moussavia G, Rahmanian O, Alipour V, Giannakis S (2020) A novel CuO/Fe_2O_3/ZnO composite for visible-light assisted photocatalytic oxidation of Bisphenol A: kinetics, degradation pathways, and toxicity elimination. Sep Purif Technol 242:116821. https://doi.org/10.1016/j.seppur.2020.116821
80. Tedla H, Díaz I, Kebede T, Taddesse AM (2015) Synthesis, characterization and photocatalytic activity of zeolite supported ZnO/Fe_2O_3/MnO_2 nanocomposites. J Environ Chem Eng 3:1586–1591. https://doi.org/10.1016/j.jece.2015.05.012
81. Pradhan GK, Martha S, Parida KM (2012) Synthesis of multifunctional nanostructured zinc–iron mixed oxide photocatalyst by a simple solution-combustion technique. ACS Appl Mater Interfaces 4:707–713. https://doi.org/10.1021/am201326b
82. Li Y, Liu K, Zhang J, Yang J, Huang Y, Tong Y (2020) Engineering the band-edge of Fe_2O_3/ZnO nanoplates via separate dual cation incorporation for efficient photocatalytic performance. Ind Eng Chem Res 59:18865–18872. https://doi.org/10.1021/acs.iecr.0c03388
83. Li C, Yu S, Che H, Zhang X, Han J, Mao Y, Wang Y, Liu C, Dong H (2018) Fabrication of Z-scheme heterojunction by anchoring mesoporous γ-Fe_2O_3 nanospheres on g-C_3N_4 for degrading tetracycline hydrochloride in water. ACS Sustain Chem Eng 6:16437–16447. https://doi.org/10.1021/acssuschemeng.8b03500
84. Babar S, Gavade N, Shinde H, Mahajan P, Lee KH, Mane N, Deshmukh A, Garadkar K, Bhuse V (2018) Evolution of waste iron rust into magnetically separable g-C_3N_4–Fe_2O_3 photocatalyst: an efficient and economical waste management approach. ACS Appl Nano Mater 1:4682–4694. https://doi.org/10.1021/acsanm.8b00936
85. Cui Y, Briscoe J, Wang Y, Tarakina NV, Dunn S (2017) Enhanced photocatalytic activity of heterostructured ferroelectric $BaTiO_3$/α-Fe_2O_3 and the significance of interface morphology control. ACS Appl Mater Interfaces 9:24518–24526. https://doi.org/10.1021/acsami.7b03523
86. Farooq U, Chaudhary P, Ingole PP, Kalam A, Ahmad T (2020) Development of uuboidal $KNbO_3$@α-Fe_2O_3 hybrid nanostructures for improved photocatalytic and photoelectrocatalytic applications. ACS Omega 5:20491–20505. https://doi.org/10.1021/acsomega.0c02646
87. Pradhan GK, Padhi DK, Parida KM (2013) Fabrication of α-Fe_2O_3 nanorod/RGO composite: a novel hybrid photocatalyst for phenol degradation. ACS Appl Mater Interfaces 5:9101–9110. https://doi.org/10.1021/am402487h
88. Shi Y, Li H, Wang L, Shen W, Chen H (2012) Novel α-Fe_2O_3/CdS cornlike nanorods with enhanced photocatalytic performance. ACS Appl Mater Interfaces 4:4800–4806. https://doi.org/10.1021/am3011516
89. Kang J, Kuang Q, Xie ZX, Zheng LS (2011) Fabrication of the SnO_2/α-Fe_2O_3 hierarchical heterostructure and its enhanced photocatalytic property. J Phys Chem C 115:7874–7879. https://doi.org/10.1021/jp111419w

90. Jana S, Mondal A (2014) Fabrication of SnO_2/α-Fe_2O_3, SnO_2/α-Fe_2O_3–PB heterostructure thin films: enhanced photodegradation and peroxide sensing. ACS Appl Mater Interfaces 6:15832–15840. https://doi.org/10.1021/am5030879
91. Sun L, Wu W, Tian Q, Lei M, Liu J, Xiao X, Zheng X, Ren F, Jiang C (2016) In situ oxidation and self-assembly synthesis of dumbbell-like α-Fe_2O_3/Ag/AgX (X = Cl, Br, I) heterostructures with enhanced photocatalytic properties. ACS Sustain Chem Eng 4:1521–1530. https://doi.org/10.1021/acssuschemeng.5b01473
92. Zhang L, Bao Z, Yu X, Dai P, Zhu J, Wu M, Li G, Liu X, Sun Z, Chen C (2016) Rational design of α-Fe_2O_3/reduced graphene oxide composites: rapid detection and effective removal of organic pollutants. ACS Appl Mater Interfaces 8:6431–6438. https://doi.org/10.1021/acsami.5b11292
93. Fu Y, Shan S, Chen F, Hu J (2020) Constructing an efficient p–n heterojunction photocatalyst $CaFe_2O_4$/Fe_2O_3 nanocomposite for degradation of methyl orange. J Mater Sci Mater Electron 31:17967–17979. https://doi.org/10.1007/s10854-020-04349-9
94. Mukhtar F, Munawar T, Nadeem MS, Hasan M, Hussain F, Nawaz MA, Iqbal F (2020) Multi metal oxide NiO–Fe_2O_3–CdO nanocomposite-synthesis, photocatalytic and antibacterial properties. Appl Phys A 126:588. https://doi.org/10.1007/s00339-020-03776-z
95. Sunkara JR, Botsa SM (2020) ZnS/Fe_2O_3/Ag ternary nanocomposite photocatalyst for the degradation of dyes under visible light. Russ J Phys Chem A 94(2):392–400. https://doi.org/10.1134/S0036024420020144
96. Mai NVN, Lim DT, Bac NQ, Chi NTH, Dung DT, Pham NN, Nhiem DN (2019) Fe_2O_3/Mn_2O_3 nanoparticles: preparations and applications in the photocatalytic degradation of phenol and parathion in water. J Chin Chem Soc 1–4. https://doi.org/10.1002/jccs.201900033
97. Sun K, Wang L, Wu C, Deng J, Pan K (2017) Fabrication of α-Fe_2O_3@rGO/PAN nanofiber composite membrane for photocatalytic degradation of organic dyes. Adv Mater Interfaces 1700845. https://doi.org/10.1002/admi.201700845
98. Huang S, Xu Y, Chen Z, Xie M, Xu H, He M, Li H, Zhang Q (2015) A core–shell structured magnetic Ag/AgBr@Fe_2O_3 composite with enhanced photocatalytic activity for organic pollutant degradation and antibacterium. RSC Adv 5:71035. https://doi.org/10.1039/c5ra13403j
99. Liu C, Wu G, Chen J, Huang K, Shi W (2016) Fabrication of a visible-light-driven photocatalyst and degradation of tetracycline based on the photoinduced interfacial charge transfer of $SrTiO_3$/Fe_2O_3 nanowires. New J Chem 40:5198–5208. https://doi.org/10.1039/c5nj03167b
100. Gao Y, Ma H, Han C, Gui C, Deng C (2022) Preparation of Ag_3PO_4/α-Fe_2O_3 hybrid powders and their visible light catalytic performances. RSC Adv 12:6328. https://doi.org/10.1039/d1ra09256a
101. Abhilash MR, Akshatha G, Srikantaswamy S (2019) Photocatalytic dye degradation and biological activities of the Fe_2O_3/Cu_2O nanocomposite. RSC Adv 9:8557. https://doi.org/10.1039/c8ra09929d
102. Bai S, Zhang K, Sun J, Luo R, Li D, Chen A (2014) Surface decoration of WO_3 architectures with Fe_2O_3 nanoparticles for visible-light-driven photocatalysis. CrystEngComm 16:3289–3295. https://doi.org/10.1039/c3ce42410c
103. Liu J, Wu W, Tian Q, Dai Z, Wu Z, Xiao X, Jiang C (2016) Anchoring of $Ag_6Si_2O_7$ nanoparticles on α-Fe_2O_3 short nanotubes as a Z-scheme photocatalyst for improving their photocatalytic performances. Dalton Trans 45:12745–12755. https://doi.org/10.1039/c6dt02499h
104. Li M, Tang Y, Shi W, Chen F, Shia Y, Gu H (2018) Design of visible-light-response core–shell Fe_2O_3/$CuBi_2O_4$ heterojunctions with enhanced photocatalytic activity towards the degradation of tetracycline: Z-scheme photocatalytic mechanism insight. Inorg Chem Front 5:3148–3154. https://doi.org/10.1039/c8qi00906f
105. Xu Y, Jing L, Chen X, Ji H, Xu H, Li H, Li H, Zhang Q (2016) Novel visible-light-driven Fe_2O_3/Ag_3VO_4 composite with enhanced photocatalytic activity toward organic pollutants degradation. RSC Adv 6:3600. https://doi.org/10.1039/c5ra22912j

106. Arul NS, Mangalaraj D, Ramachandran R, Gracec AN, Han JI (2015) Fabrication of CeO_2/Fe_2O_3 composite nanospindles for enhanced visible light driven photocatalysts and supercapacitor electrodes. J Mater Chem A 3:15248–15258. https://doi.org/10.1039/c5ta02630j
107. Li N, Hua X, Wang K, Jin Y, Xu J, Chen M, Teng F (2014) In situ synthesis of uniform Fe_2O_3/BiOCl p/n heterojunctions and improved photodegradation properties for mixture dyes. Dalton Trans 43:13742–13750. https://doi.org/10.1039/c4dt01999g
108. Kanwal A, Sajjad S, Leghari SAK, Yousaf Z (2021) Cascade electron transfer in ternary CuO/α-Fe_2O_3/γ-Al_2O_3 nanocomposite as an effective visible photocatalyst. J Phys Chem Solids 151:109899. https://doi.org/10.1016/j.jpcs.2020.109899
109. Botsa SM, Naidu GP, Ravichandra M, Rani SJ, Anjaneyulu RB, Ramana ChV (2020) Flower like SnO_2–Fe_2O_3–rGO ternary composite as highly efficient visible light induced photocatalyst for the degradation of organic pollutants from contaminated water. J Mater Res Technol 9(6):12461–12472. https://doi.org/10.1016/j.jmrt.2020.08.087
110. Ma C, Lee J, Kim Y, Seo WC, Jung H, Yang W (2021) Rational design of α-Fe_2O_3 nanocubes supported $BiVO_4$ Z-scheme photocatalyst for photocatalytic degradation of antibiotic under visible light. J Colloid Interface Sci 581:514–522. https://doi.org/10.1016/j.jcis.2020.07.127
111. Zhang R, Liu S, Kong F, Tong J, Ruan L, Duan Q, Zhou J, Zhang X (2020) α-Fe_2O_3/$BiFeO_3$ composites as visible-active photocatalysts and their optical response mechanism. J Phys Chem Solids 141:109329. https://doi.org/10.1016/j.jpcs.2019.109329
112. Wang H, Wang C, Cui X, Qina L, Ding R, Wang L, Liu Z, Zheng Z, Lv B (2018) Design and facile one-step synthesis of $FeWO_4/Fe_2O_3$ di-modified WO_3 with super high photocatalytic activity toward degradation of quasiphenothiazine dyes. Appl Catal B 221:169–178. https://doi.org/10.1016/j.apcatb.2017.09.011
113. Tian B, Wang T, Dong R, Bao S, Yang F, Zhang J (2014) Core–shell structured α-Fe_2O_3@SiO_2@AgBr: Ag composite with high magnetic separation efficiency and excellent visible light activity for acid orange 7 degradation. Appl Catal B 147:22–28. https://doi.org/10.1016/j.apcatb.2013.08.028
114. Zhang H, Li M, Cao J, Tang Q, Kang P, Zhu C, Ma M (2018) 2D α-Fe_2O_3 doped Ti_3C_2 MXene composite with enhanced visible light photocatalytic activity for degradation of Rhodamine B. Ceram Int 44:19958–19962. https://doi.org/10.1016/j.ceramint.2018.07.262
115. Zhang R, Du B, Li Q, Cao Z, Feng G, Wang X (2019) α-Fe_2O_3 nanoclusters confined into UiO-66 for efficient visible-light photodegradation performance. Appl Surf Sci 466:956–963. https://doi.org/10.1016/j.apsusc.2018.10.048
116. Helal A, Harraz FA, Ismail AA, Sami TM, Ibrahim IA (2017) Hydrothermal synthesis of novel heterostructured Fe_2O_3/Bi_2S_3 nanorods with enhanced photocatalytic activity under visible light. Appl Catal B Environ 213:18–27. https://doi.org/10.1016/j.apcatb.2017.05.009
117. Niu J, Zhang Z, Dai P, Yao B, Yu X, Zhang Q, Yang R (2018) Facile synthesis of γ-Fe_2O_3/BiOI microflowers with enhanced visible light photocatalytic activity. Mater Des 150:29–39. https://doi.org/10.1016/j.matdes.2018.04.001
118. Guo R, Qi X, Zhang X, Zhang H, Cheng X (2019) Synthesis of Ag_2CO_3/α-Fe_2O_3 heterojunction and it high visible light driven photocatalytic activity for elimination of organic pollutants. Sep Purif Technol 211:504–513. https://doi.org/10.1016/j.seppur.2018.10.011
119. Liu Q, Cao J, Jia Y, Li X, Li W, Zhu Y, Liu X, Li J, Yang J, Yang Y (2020) Construction of a direct Z-scheme ZnS quantum dot (QD)-Fe_2O_3 QD heterojunction/reduced graphene oxide nanocomposite with enhanced photocatalytic activity. Appl Surf Sci 506:144922. https://doi.org/10.1016/j.apsusc.2019.144922
120. Lv SW, Liu JM, Zhao N, Li CY, Yang FE, Wang ZH, Wang S (2020) MOF-derived $CoFe_2O_4$/Fe_2O_3 embedded in g-C_3N_4 as high-efficient Z scheme photocatalysts for enhanced degradation of emerging organic pollutants in the presence of persulfate. Sep Purif Technol 253:117413. https://doi.org/10.1016/j.seppur.2020.117413
121. Zhu H, Chen Z, Hu Y, Gong L, Li D, Li Z (2020) A novel immobilized Z-scheme P3HT/α-Fe_2O_3 photocatalyst array: study on the excellent photocatalytic performance and photocatalytic mechanism. J Hazard Mater 389:122119. https://doi.org/10.1016/j.jhazmat.2020.122119